AGU PUBLICATIONS

JGR

Journal of Geophysical Research: Space Physics

RESEARCH ARTICLE
10.1002/2016JA022523

Special Section:
Big Storms of the Van Allen Probes Era

The dependence on geomagnetic conditions and solar wind dynamic pressure of the spatial distributions of EMIC waves observed by the Van Allen Probes

A. A. Saikin[1], J.-C. Zhang[1], C. W. Smith[1], H. E. Spence[1], R. B. Torbert[1], and C. A. Kletzing[2]

[1]Space Science Center and Department of Physics, University of New Hampshire, Durham, New Hampshire, USA, [2]Department of Physics and Astronomy, University of Iowa, Iowa City, Iowa, USA

Key Points:
- EMIC waves are examined with varying levels of dynamic pressure and geomagnetic indices
- During quiet ($AE \leq 100$ nT) activity levels, the prenoon sector features high occurrence rates
- For active periods (storms or substorms), the afternoon sector displays highest occurrence rates

Correspondence to:
A. A. Saikin,
aax75@wildcats.unh.edu

Citation:
Saikin, A. A., J.-C. Zhang, C. W. Smith, H. E. Spence, R. B. Torbert, and C. A. Kletzing (2016), The dependence on geomagnetic conditions and solar wind dynamic pressure of the spatial distributions of EMIC waves observed by the Van Allen Probes, *J. Geophys. Res. Space Physics*, *121*, 4362–4377, doi:10.1002/2016JA022523.

Received 9 FEB 2016
Accepted 27 APR 2016
Accepted article online 29 APR 2016
Published online 20 MAY 2016

Abstract A statistical examination on the spatial distributions of electromagnetic ion cyclotron (EMIC) waves observed by the Van Allen Probes against varying levels of geomagnetic activity (i.e., *AE* and *SYM-H*) and dynamic pressure has been performed. Measurements taken by the Electric and Magnetic Field Instrument Suite and Integrated Science for the first full magnetic local time (MLT) precession of the Van Allen Probes (September 2012–June 2014) are used to identify over 700 EMIC wave events. Spatial distributions of EMIC waves are found to vary depending on the level of geomagnetic activity and solar wind dynamic pressure. EMIC wave events were observed under quiet ($AE \leq 100$ nT, 325 wave events), moderate ($100\,\text{nT} < AE \leq 300$ nT, 218 wave events), and disturbed ($AE > 300$ nT, 228 wave events) geomagnetic conditions and are primarily observed in the prenoon sector ($\sim 800 < \text{MLT} \leq \sim 1100$) at $L \approx 5.5$ during quiet activity times. As *AE* increases to disturbed levels, the peak occurrence rates shift to the afternoon sector ($1200 < \text{MLT} \leq 1800$) between $L = 4$ and $L = 6$. A majority of EMIC wave events (~56%) were observed during nonstorm times (defined by *SYM-H*). Consistent with the quiet *AE* levels, nonstorm EMIC waves are observed in the prenoon sector. EMIC waves observed through the duration of a geomagnetic storm are primarily located in the afternoon sector. High solar wind pressure (Pdyn > 3 nPa) correlates to mostly afternoon EMIC wave observations.

1. Introduction

Electromagnetic ion cyclotron (EMIC) waves are Pc 1-2 pulsations (frequency ranges 0.1–5 Hz) that are generated with a left-handed polarization [*Rauch and Roux*, 1982]. Once generated, EMIC waves propagate away from their source regions to areas of increased magnetic field strength [*Mauk and McPherron*, 1980]. EMIC waves impact particle dynamics and cross-energy plasma interactions within the Earth's magnetosphere. These interactions consist of relativistic electron pitch angle scattering [*Thorne and Kennel*, 1971; *Lyons et al.*, 1972; *Summers and Throne*, 2003; *Summers et al.*, 2007; *Jordanova et al.*, 2008], heavy ion heating [*Zhang et al.*, 2010, 2011], and energetic proton scattering loss in the ring current [*Jordanova et al.*, 2001]. EMIC waves are also correlated with the appearance of isolated auroral arc events [*Sakaguchi et al.*, 2008] and may cause traveling convection vortices in the Earth's magnetosphere [*Lockwood et al.*, 1990; *Engebretson et al.*, 2013].

EMIC wave generation hinges on the availability of hot (10–100 keV) anisotropic ($T_\perp > T_\parallel$) ions (typically in the ring current) to overlap with a cold dense plasma population [*Cornwall*, 1965; *Kennel and Petschek*, 1966]. The hot ion population provides the free energy necessary for EMIC waves to generate [*Cornwall*, 1965; *Rauch and Roux*, 1982], while the cold plasma population increases the wave growth rate [*Young et al.*, 1981; *Rauch and Roux*, 1982; *Horne and Thorne*, 1993]. The cold dense plasma populations necessary for EMIC wave generation may be supplied by the plasmasphere or plasmaspheric plumes [*Fraser et al.*, 1989; *Horne and Thorne*, 1993; *Morley et al.*, 2009; *Pickett et al.*, 2010]. During geomagnetic storms, energetic ring current ions can be injected deeper into the inner magnetosphere where they can overlap with the cold plasmasphere ion populations allowing EMIC waves to generate [*Cornwall*, 1965; *Criswell*, 1969; *Jordanova et al.*, 2001; *Fraser et al.*, 2010]. Observations made by the Combined Release and Radiation Effects Satellite (CRRES) mission show that most EMIC wave events were observed in the duskside plasma bulge region [*Fraser and Nguyen*, 2001]. Further

work shows that EMIC waves are up to ~20 times more likely to be observed inside a plasmaspheric plume than outside [*Usanova et al.*, 2013].

EMIC waves are preferably generated in regions of low magnetic field strength [*Kennel and Petschek*, 1966]. By utilizing the CRRES mission, the location of bidirectional EMIC wave events, which are typically observed within the source region, were found to be confined within ±11° magnetic latitude (MLAT) of the magnetic equator [*Loto'aniu et al.*, 2005]. If we assume a dipole magnetic field, these near equatorial source regions coincide with where magnetic field magnitude minima are located. EMIC wave generation, however, is not exclusive to the magnetic equator. Bidirectional EMIC waves have been observed within the 30°–45° MLAT range [*Allen et al.*, 2013]. Off equator source regions may be attributed to magnetospheric compressions caused by increases in the solar wind dynamic pressure which disturbs plasma [*Olson and Lee*, 1983; *Bräysy et al.*, 1998] and allow particles to execute Shabansky orbits on the dayside [*McCollough et al.*, 2012; *Allen et al.*, 2015].

Statistical studies, ranging from $L = 1$ to $L = 15$, have reported EMIC wave observations throughout all magnetic local times (MLTs) and L shells [*Anderson et al.*, 1992; *Kasahara et al.*, 1992; *Halford et al.*, 2010; *Min et al.*, 2012; *Usanova et al.*, 2012; *Keika et al.*, 2013; *Meredith et al.*, 2014; *Allen et al.*, 2015; *Yu et al.*, 2015; *Saikin et al.*, 2015; *Wang et al.*, 2015]. EMIC waves are consistently observed in the afternoon sector (~1200 < MLT ≤ ~1800), where plasmaspheric plumes are known to exist [*Anderson et al.*, 1992; *Halford et al.*, 2010; *Min et al.*, 2012; *Usanova et al.*, 2012, 2013; *Keika et al.*, 2013; *Meredith et al.*, 2014; *Saikin et al.*, 2015]. Dawn sector (~300 < MLT ≤ ~900) EMIC wave occurrence peaks are also observed in the outer magnetosphere ($L \geq$ ~10) [*Min et al.*, 2012; *Usanova et al.*, 2012; *Allen et al.*, 2015].

To further our understanding how EMIC waves can influence the magnetosphere, we must understand the conditions under which they can generate and how the variation of these conditions impacts the spatial distributions of EMIC waves. Previous statistical studies have explored the relationship to geomagnetic indices and solar wind conditions over different regions of the magnetosphere. Each study examined EMIC waves with measurements from a different mission, with its own respective orbits and main regions of focus, giving a more global understanding of how EMIC waves generate in relation to geomagnetic and solar wind conditions. Observations by the Charge Composition Explorer (CCE) spacecraft in the Active Magnetopsheric Particle Tracer Explorers (AMPTE) mission explored the correlation between EMIC waves with respect to *Dst* [*Keika et al.*, 2013]. This study incorporated H^+ and He^+ band EMIC wave observations and concluded that band-specific EMIC wave occurrence peaks were each related to different trigger mechanisms. The dayside H^+ band occurrence peaks were found to be associated with dayside compressions, while the afternoon sector He^+ band occurrence peaks were more correlated with the injections of energetic ion populations. The majority of the measurement coverage reported by *Keika et al.* [2013], despite being roughly equally covered in MLT, are focused between $L = 7$ and $L = 9$. While EMIC wave observations are reported below $L = 7$, the data coverage is still disproportionally in favor of the $L > 7$ regions.

Conversely, observations by the Akebono satellite, launched in February 1989, do not showcase a clear dependence between band-specific EMIC waves and geomagnetic activity [*Kasahara et al.*, 1992]. The Akebono satellite has an apogee and perigee of 10,500 km and 275 km, respectively, which allows for the exploration of very low L shells within the Earth's magnetosphere. Using only data coverage during geomagnetic equatorial crossings, Akebono observed both H^+ and He^+ band EMIC waves between $L = 1$ and $L = 3$. By examining the occurrence rates of H^+ and He^+ band EMIC waves against the *Kp* index, *Kasahara et al.* [1992] found that high *Kp* values ($Kp > 7$) yielded higher occurrence rates of EMIC waves. However, the preference for observances of exclusively H^+ or He^+ band EMIC wave events or both bands observed simultaneously could not be distinguished.

Operated from July 1990 to September 1991, the CRRES mission was designed to explore the inner magnetosphere, with a perigee and apogee of 350 km and 6.3 R_E, respectively. *Halford et al.* [2010] performed a statistical study of EMIC waves observed by CRRES in relation to storm phase as determined by *SYM-H*. Their results indicated that the afternoon sector had the highest occurrence rates of EMIC waves during both the main and recovery phases of geomagnetic storms. Another analysis using the CRRES data set examined EMIC wave occurrence, by wave band, against the auroral electrojet (*AE*) index [*Meredith et al.*, 2014]. This study found that under disturbed ($AE > 300$ nT) geomagnetic conditions, both H^+ and He^+ band EMIC wave events had higher occurrence rates in the afternoon sector. Note that CRRES never managed to complete a full MLT precession around the Earth. As a result, there remains a noticeable gap in data coverage between 800 and 1400 MLTs.

Outer magnetosphere EMIC waves have been examined using measurements from the Time History of Events and Macroscale Interactions during Substorms (THEMIS) [*Min et al*., 2012; *Usanova et al*., 2012]. EMIC wave events have been cross examined under the *AE*, *SYM-H*, and *Kp* indices as well as solar wind dynamic pressure [*Usanova et al*., 2012]. *Usanova et al.* [2012] found that, similar to that by *Meredith et al.* [2014], occurrence rates of afternoon sector EMIC waves increased under disturbed ($AE > 300$ nT) geomagnetic conditions. Peak occurrence rates of dawn centered EMIC waves were correlated with dayside compressions of the magnetosphere (Pdyn > 3 nPa and *SYM-H* > 0 nT). This result concurs with previous case studies [*Anderson and Hamilton*, 1993; *Fuselier et al*., 2004], and theoretical models which posit that dayside compression of the magnetosphere can lead to particles executing the Shabansky orbits [*Shabansky*, 1971], thereby creating the necessary anisotropic plasma populations for EMIC wave generation in off-equator regions in the outer magnetosphere [*Tsurutani and Smith*, 1977; *McCollough et al*., 2012]. *Usanova et al.* [2012] made no distinction between H^+ and He^+ band EMIC waves. While THEMIS has data coverage below $L = 6$, EMIC waves were scarcely observed in the inner magnetosphere [*Min et al*., 2012; *Usanova et al*., 2012].

Launched in August 2012, the Van Allen Probes have provided more opportunities to explore EMIC waves in the radiation belts and the inner magnetosphere [*Zhang et al*., 2014; *Engebretson et al*., 2015; *Saikin et al*., 2015; *Wang et al*., 2015; *Yu et al*., 2015]. The MLT sectors that were previously underexplored at those *L* shells by the CRRES mission now have sufficient data coverage [*Saikin et al*., 2015]. Studies revealed the existence of prenoon ($800 < \mathrm{MLT} \leq 1100$) occurrence peaks for the H^+, He^+, or O^+ band EMIC waves [*Saikin et al*., 2015; *Wang et al*., 2015; *Yu et al*., 2015]. The solar wind conditions or the geomagnetic activity associated with these prenoon EMIC wave events have only been examined in a case study [*Engebretson et al*., 2015]. A large-scale statistical study relating how all inner magnetosphere EMIC waves are connected to geomagnetic activity or solar wind parameters is needed to understand the generation mechanisms involved, especially with this newly revealed prenoon peak occurrence region.

The present study presents an examination of EMIC waves in the inner magnetosphere detected by both of the Van Allen Probes over the first 22 month period of the mission with geomagnetic activity levels and solar wind conditions. The paper will be presented in the following manner: a description of the Van Allen Probes and instrumentation used (section 2.1), the indices used to monitor and define geomagnetic activity levels and solar wind dynamic pressure (section 2.2), results on the spatial distributions of EMIC waves based by geomagnetic activity and solar wind dynamic pressure (sections 3.1–3.3), a description of the current solar cycle (section 3.4), and finally discussion and conclusions (sections 4 and 5, respectively).

2. Instrumentation and Technique

2.1. Van Allen Probes

The Van Allen Probes mission [*Kessel et al*., 2013; *Mauk et al*., 2013] consists of two identical spacecraft that orbit around the Earth between a perigee and apogee of 1.1 and 5.8 R_E, respectively. Both probes have an orbital period of ~9 h and follow a low inclination (~10°), highly elliptical orbit. The perigee-apogee line of each probe, i.e., the line of apsides, precesses in local time at a rate of ~210° per year. The probes, denoted as A and B, follow nearly identical trajectories at different speeds such that one probe laps the other every ~2.5 months.

Our EMIC wave selection criteria follow the method described in *Saikin et al.* [2015] (see section 2.2 and Figure 1 of *Saikin et al.* [2015]). High-resolution magnetic field data taken by the Van Allen Probes' Electric and Magnetic Field Instrument Suite and Integrated Science (EMFISIS) instrument [*Kletzing et al*., 2013] during the Van Allen Probes' first precession (8 September 2012–30 June 2014) were processed through the fast Fourier transform technique. Daily plots of EMFISIS data were generated from which EMIC waves events were identified visually. For each wave event the wave start time and the wave end time were documented on a wave event list. Broadband wave activity was not identified as an EMIC wave event (see *Zhang et al.* [2014] for an example of EMIC wave activity and broadband wave activity). Each wave event must have been observed for at least 5 min in universal time (UT) to avoid being considered background noise. Furthermore, EMIC wave events were identified using a minimum wave power threshold of 0.01 nT^2/Hz. Wave power was calculated following the method described in *Allen et al.* [2013] and *Zhang et al.* [2014]. EMIC wave activity was included in this study if the wave activity was observed at a frequency higher than 0.1 Hz but lower than the local proton gyrofrequency. This frequency range allowed us to include proton, helium, and oxygen band EMIC

wave events. An analysis examining band separation, geomagnetic indices, and dynamic pressure has not been performed as part of this study.

2.2. Geomagnetic Indices and Dynamic Pressure

For this study, EMIC wave events were examined against the *AE*, *SYM-H*, and solar wind dynamic pressure. This study used the 5 min OMNI resolution data set. Given the location of the bow shock [*Merka et al*., 2003], it could take an estimated 3–5 min for the solar wind to reach the location of the Van Allen Probes. The use of the 5 min OMNI resolution data set allows us to include a one data point time delay shift with regards to solar wind dynamic pressure. No additional time delay has been incorporated for the *AE* or *SYM-H* measurements beyond how the OMNI data set is already shifted (i.e., to the bow shock nose). The *AE* index was used to examine EMIC wave occurrence with substorm activity. To be consistent with previous studies [*Usanova et al*., 2012; *Meredith et al*., 2014], *AE* was divided into three classes: quiet ($AE \leq 100$ nT), moderate ($100\ \text{nT} < AE \leq 300$ nT), and disturbed ($AE > 300$ nT) activity conditions. These geomagnetic activity level definitions were then used to determine the data coverage of the Van Allen Probes for each respective condition. Figure 1 shows a sample geomagnetic storm beginning on 7 May 2014 and ending on 9 May 2014. The top three plots showcase the *AE* index (Figure 1a), the *SYM-H* index (Figure 1b), and the dynamic pressure (Figure 1c) before, after, and through the duration of the storm. A few proton band EMIC wave events observed during this storm have also been included (Figure 1d). During this particular storm, the *AE* index (Figure 1a) varies from ~50 nT (quiet geomagnetic activity) to 750 nT (disturbed geomagnetic activity). Each green vertical line represents the start time of an EMIC wave event observed and has been mapped appropriately to Figure 1d. The dashed green lines in Figure 1d denote the end of those EMIC wave events. The events were observed on 8 May 2015 from 10:01 to 10:15 UT and 9 May 2015 from 20:40 to 20:51 UT, 21:04 to 21:30 UT, and 21:41 to 22:31 UT, respectively. All EMIC waves observed during this storm were under moderate or quiet geomagnetic conditions.

Storms and storm phases were defined and categorized in the same manner as *Halford et al.* [2010]. *SYM-H* was determined to be the preferred index over *Dst* due to the higher resolution of the *SYM-H* data (5 min resolution data was used, averaged from the original 1 min data) compared to *Dst* (1 h resolution). This high-resolution *SYM-H* index allows for more accurate classifications of nonstorm and storm time phases (i.e., preonset, main, and recovery phases) in relation to when EMIC wave events are observed. To be defined as a geomagnetic storm, the minimum *SYM-H* index must reach a value of −40 nT. The main phase of the storm was determined to begin at the moment when the slope of the *SYM-H* index turns negative (the blue dash-dotted vertical line in Figure 1b), while reaching the −40 nT threshold. Upon reaching the minimum *SYM-H* value (the pink dash-dotted vertical line in Figure 1b), the main phase ends and the recovery phase begins. The recovery phase was determined to conclude when the *SYM-H* index had reached 20% of the minimum *SYM-H* value (the red dash-dotted vertical line in Figure 1b). To be consistent with *Halford et al.* [2010], the preonset phase was defined as 3 h before the onset of the main phase (the black dash-dotted vertical line in Figure 1b). For reference, the solid gold line on Figure 1b denotes $SYM\text{-}H = 0$ nT. All EMIC wave events associated with this particular storm activity are observed in the recovery phase.

EMIC wave observations were also examined against the solar wind dynamic pressure. Figure 1c shows the variation of dynamic pressure during the 7 May 2014 storm. Prior to the beginning of the main phase, dynamic pressure remains under 1 nPa. During the main phase of the storm the dynamic pressure dramatically increases to over 2 nPa. The dynamic pressure peaks around ~5 nPa during the recovery phase and continues to remain above 1 nPa for the duration of the storm. All EMIC wave events occur when the pressure is less than 3 nPa. As previously mentioned, no time delay was included when examining EMIC wave events in relation to solar wind dynamic pressure. Since we have used the 5 min resolution data set, time delays would only consist of, at most, a one or two data point shift. Given this small shift, the authors have not felt it necessary to include a time delay factor for the solar wind dynamic pressure.

3. Observational Results

3.1. EMIC Waves by *AE*

The following plots incorporate data observations taken from both Van Allen Probes, A and B. The bin sizes represent 15 min of MLT per 0.5 *L* shell. This resolution was chosen to remain consistent with *Saikin et al.* [2015]. We used the 2004 Tsyganenko and Sitnov magnetic field model (TS04D) [*Tsyganenko and Sitnov*,

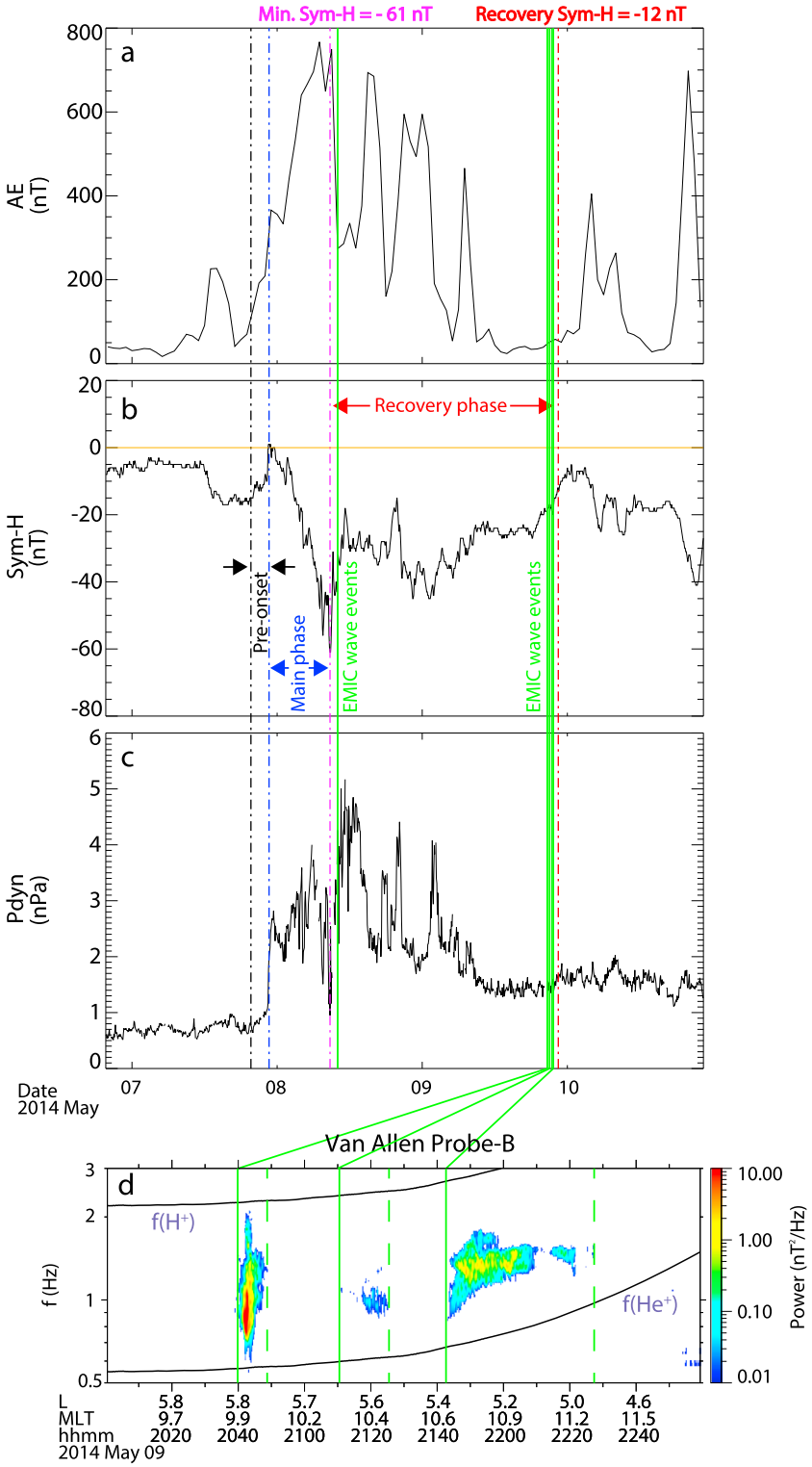

Figure 1. A sample geomagnetic storm observed from 7 May 2014 to 9 May 2014. Displayed are (a) *AE*, (b) *SYM-H*, (c) dynamic pressure, and (d) a few proton-band EMIC wave events observed during this storm. The lines represent the start of the preonset phase (black vertical dashed line), the start of the main phase of the storm (blue vertical dashed line), the point of minimum *SYM-H* (pink vertical dashed line), and the end of the recovery phase (red vertical dashed line). Green vertical lines denote the start of an EMIC wave event observation and have been mapped to correspond to their respective event in Figure 1d. The dashed green lines denote the end of the EMIC wave event. The horizontal line denotes *SYM-H* = 0 nT (gold solid line). The curved black lines in Figure 1d denote that respective ion gyrofrequency.

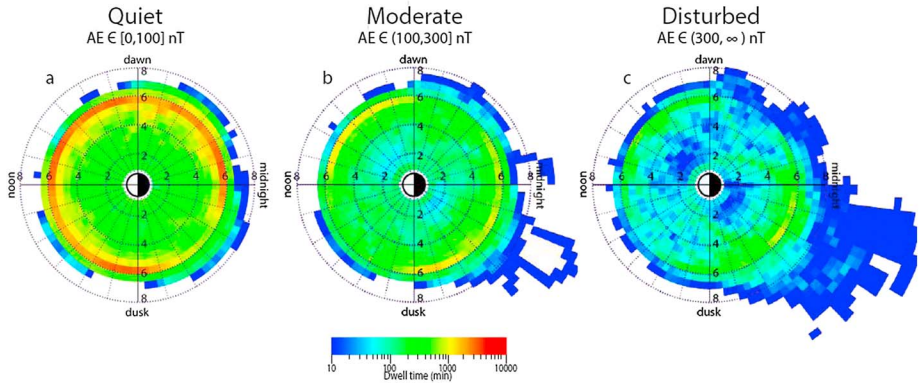

Figure 2. The data coverage of the Van Allen Probes under (a) quiet, (b) moderate, and (c) disturbed geomagnetic conditions as defined by the *AE* index. Each cell refers to 15 min in MLT per half *L* shell. Overplotted on this plot are circles representing the $L = 2$, 4, 6, and 8 shell, respectively.

2005] to calculate the *L* values. White regions denote areas where the Van Allen Probes do not have magnetic field measurements. The Van Allen Probes' data coverage has been divided over the three aforementioned geomagnetic conditions (quiet, moderate, and disturbed) as determined by the *AE* index. Figure 2 shows the data coverage of the Van Allen Probes using these definitions. Throughout the first full precession of the Van Allen Probes, a majority of the mission has taken data under quiet geomagnetic conditions, as shown in Figure 2a. As the *AE* value increases, the amount of dwell time decreases. The moderate and disturbed *AE* condition data coverage plots (Figures 2b and 2c, respectively) feature increased dwell time in the prenoon (~600 < MLT < ~1200) and premidnight (~1800 < MLT < ~2400) sectors around $L = \sim 6$. Furthermore, primarily on the disturbed data coverage plot (Figure 2c), the Van Allen Probes' observations extend as high as $L = 14$. The Van Allen Probes never go beyond their 5.8 R_E apogee. This high *L* shell data coverage is caused by TS04D model reacting to the increased geomagnetic activity, during which off-equator probe locations are mapped to high equatorial distances from the center of the Earth. Figure 2 shows that the $L \leq 6$ dwell time is generally >100 min, which will only be used to designate "sufficient dwell time" for the occurrence rates determined by the *AE* index.

EMIC wave occurrence rates were determined in the same manner as *Saikin et al.* [2015]. The time duration of each wave packet has been catalogued and summed within each respective bin of MLT and *L* shell. Furthermore, EMIC wave events were categorized by the geomagnetic condition under which they were observed. The occurrence rate is then defined as the total amount of EMIC wave observation time divided

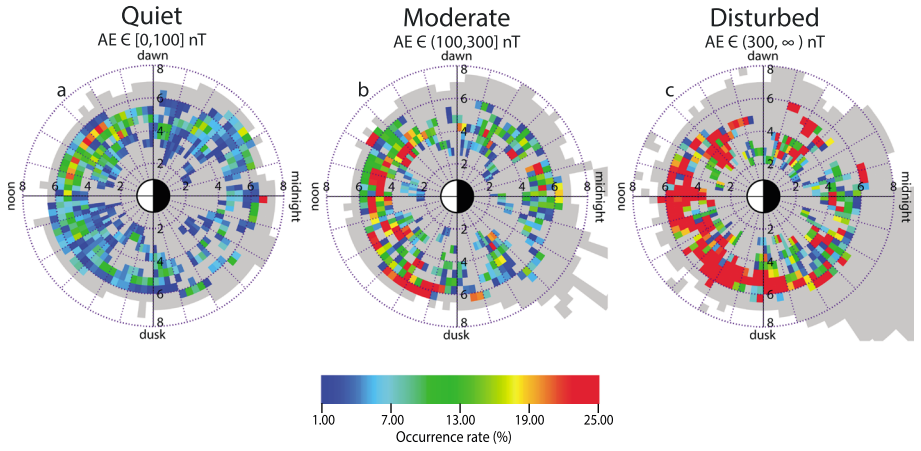

Figure 3. Same format as in Figure 2 but showing the occurrence rates of all EMIC waves observed by the Van Allen Probes from 8 September 2012 to 30 June 2014 based on the geomagnetic condition (as defined by the *AE* index) during which they were observed. Each occurrence plot is normalized to its respective condition's data coverage. Grey areas refer to the regions where the Van Allen Probes were located but did not observe EMIC wave activity.

Table 1. EMIC Wave Occurrence by *AE* Index

	Quiet	Moderate	Disturbed
EMIC wave events	325	218	228
Hours of EMIC activity	193.14	137.49	124.15
Percentage of total dwell time	1.00%	1.63%	2.84%

by the amount of dwell time that the Van Allen Probes have in that bin under that geomagnetic activity level. Figure 3 shows the occurrence rates of EMIC waves observed by the Van Allen Probes over the first 22 months of the mission with respect to geomagnetic activity as determined by *AE*. Grey regions represent where the Van Allen Probes have data coverage yet observed no EMIC wave activity, regardless whether the dwell time was sufficient. All events are displayed in Figure 3. If a region is not explicitly mentioned in the text where EMIC waves were observed, then that region did not satisfy our sufficient dwell time definition. Table 1 shows the breakdown of the number of EMIC wave events which were observed under each respective condition. Most observations of EMIC waves occurred when geomagnetic activity levels were quiet (325 EMIC wave events, ~193 h of EMIC wave activity). Under quiet activity levels (Figure 3a), there exists a prenoon (~800 < MLT ≤ ~1100 at $L \approx 5.5$) occurrence peak. Despite having a prenoon occurrence peak, there is an overall symmetric MLT distribution of EMIC waves with the premidnight sector (~1900 < MLT ≤ ~2400) having the lowest occurrence rates and the sparsest spatial distribution. Occurrence rates at low *L* shells ($L \leq 4$) are consistently under 13%.

As *AE* increases to moderate geomagnetic activity levels (Figure 3b), the location of the peak occurrence regions shifts from the prenoon sector to an overall dayside (~800 < MLT ≤ ~1700) region while primarily at $L \geq 4$. The premidnight sector still remains spatially sparse. Overall, there were 218 EMIC wave event observations (~137 h of EMIC wave activity) when geomagnetic activity was considered moderate.

Under disturbed geomagnetic conditions, 228 EMIC wave events (~123 h of EMIC wave activity) were observed. The peak occurrence rates (~25%) of disturbed EMIC waves (Figure 3c) is concentrated almost exclusively in the afternoon sector (1200 < MLT ≤ 1800) at $L = 4$–6. Unlike the previous geomagnetic conditions, the distribution of disturbed EMIC waves has more prevalence in the midnight sector. Furthermore, at higher *AE* levels there are increased occurrence rates at lower *L* shells ($L \leq 4$) when compared to the quiet or moderate activity levels.

3.2. EMIC Waves by Storm Phase

Using the definitions described in section 2, the Van Allen Probes data coverage has been divided between nonstorm time and storm time (Figure 4). Here we have defined storm time as the time from the start of the preonset phase to the end of the recovery phase. Figure 4a shows the data coverage for nonstorm time

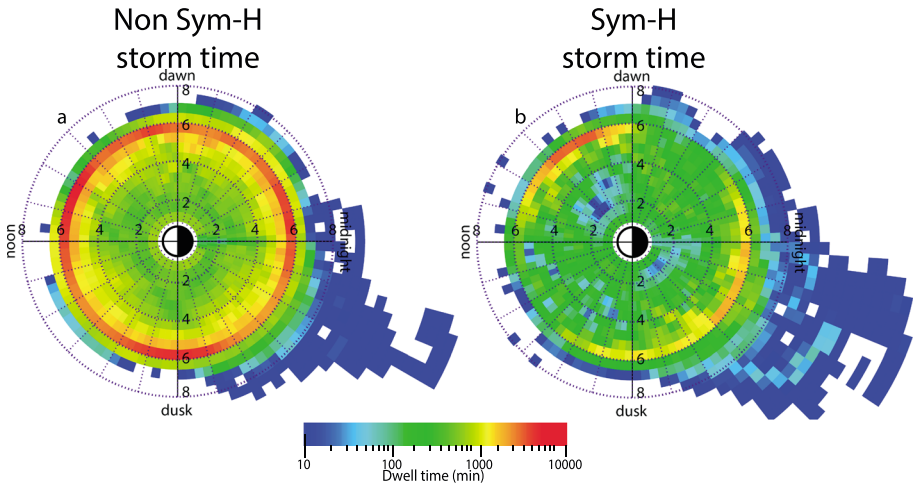

Figure 4. The data coverage of the Van Allen Probes under (a) non *SYM-H* storm time and (b) *SYM-H* storm time as determined by the *SYM-H* value. Storm time is defined as the beginning of the preonset phase to the end of the recovery phase.

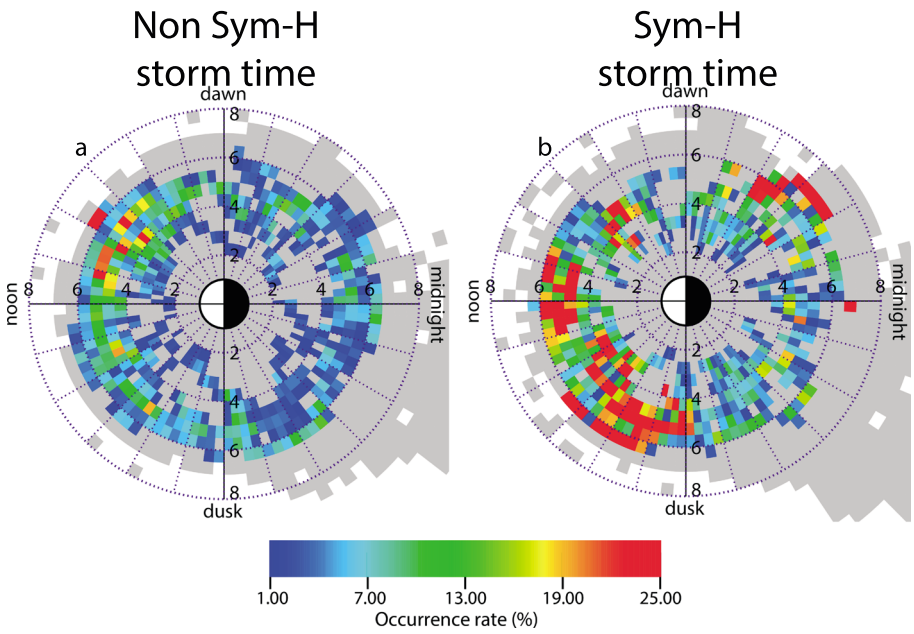

Figure 5. Same format as in Figure 4 but showing the occurrence rates of all EMIC waves observed by the Van Allen Probes based on the storm condition (as determined by the *SYM-H* value) in which they were observed.

during the Van Allen Probes' first precession. Similar to the moderate and disturbed geomagnetic activity data coverage plots (Figures 2b and 2c), dwell time during the storm time plot (Figure 4b) is increased in the prenoon and premidnight sector. The same definition of sufficient dwell time used with the *AE* index has also been applied here. There were a total of 73 storms during the first precession of the Van Allen Probes.

The occurrence plot of nonstorm EMIC waves is displayed in Figure 5a. Table 2 provides a breakdown on the EMIC wave distribution by storm phase. Overall a majority of EMIC wave events were observed during nonstorm time (432 EMIC wave events, ~264 h of EMIC wave activity). Throughout the first precession of the Van Allen Probes, ~27,481 h of observations did not coincide with any storm activity. When normalized to total nonstorm dwell time, EMIC wave observations account for ~0.96% of total observations. The spatial distribution of nonstorm EMIC waves is fairly uniform in MLT. There is a peak occurrence region in the prenoon sector ($800 < \mathrm{MLT} \leq 1100$ around $L \approx 5$). This is roughly the same region where peak EMIC wave occurrence was located for quiet geomagnetic activity. The premidnight sector shows the lowest occurrence rates.

Between the three storm phases (preonset, main, and recovery), a majority of the storm time EMIC wave events were observed in the recovery phase (218 EMIC wave events, ~119 h of EMIC wave activity). Main phase EMIC wave events comprised a total of 93 event observations totaling ~54 h of EMIC wave activity. The preonset EMIC waves showcase the least amount of EMIC wave observations (29 EMIC wave events, ~17 h of EMIC wave activity). During the 73 storms of the first precession, Van Allen Probes storm dwell time totaled ~3599 h (219 h from the preonset, ~1322 h from the main phase, and ~2058 h from the recovery phase). That is, a majority of the storm time EMIC wave events have been observed in the recovery phase. EMIC wave activity accounts for ~5.76% of the total recovery dwell time. EMIC wave activity observed in the main phase accounts for ~4.13% of the total main phase dwell time. The preonset phase marks the highest percentage of total dwell time of the three phases (7.9%).

Table 2. EMIC Wave Occurrence by the Storm Phases as Defined by *SYM-H*

	Prestorm	Main Phase	Recovery Phase	Total Storm	Nonstorm
EMIC wave events	28	93	218	339 (~44%)[a]	432 (~56%)[a]
Hours of EMIC activity	17.35	54.58	118.53	190.46	264.32
Percentage of total dwell time	7.9%	4.13%	5.76%	5.29%	0.96%

[a]Percentage out of total EMIC wave events observed.

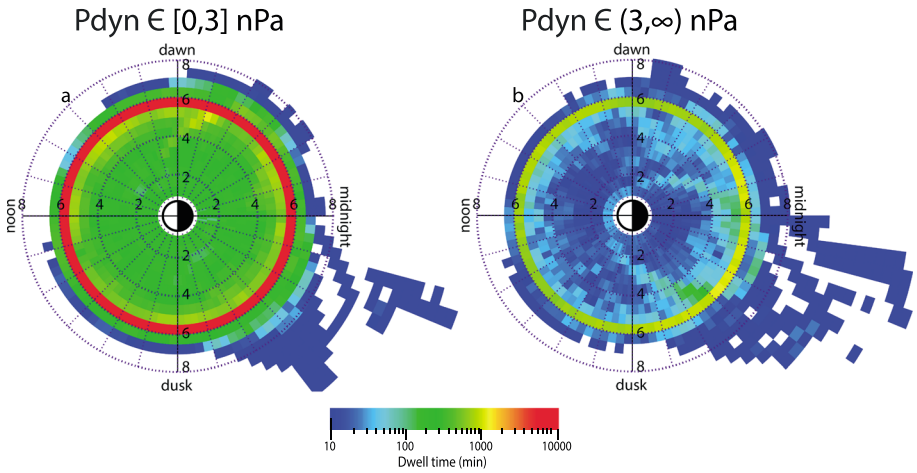

Figure 6. The data coverage of the Van Allen Probes under (a) low-pressure (Pdyn $\leq$ 3 nPa) conditions and (b) high-pressure (Pdyn $>$ 3 nPa) conditions.

The distribution of storm time EMIC waves is displayed in Figure 5b. A breakdown of EMIC wave occurrence by storm phase (i.e., preonset versus main versus recovery) very closely reflected the result displayed in Figure 5b with regards to spatial distribution and therefore have not been included. Furthermore, since the dwell time distribution is uneven among the three phases, storm phase-specific plots would produce more nonsufficient data coverage bins. Despite having less dwell time coverage, the afternoon sector still shows higher occurrence rates than any other sector, primarily beyond $L = 4$. This is consistent with previous studies which showed more EMIC wave events in the afternoon sector during storm time [*Halford et al*., 2010; *Keika et al*., 2013]. Higher occurrence rates are also observed at lower L ($L < 4$) shells when compared to the nonstorm time occurrence plot, with occurrence rates increases from ~1% to ~7%. Even at lower L shells the afternoon sector still produces higher occurrence rates (some around ~25%) than any other MLT sectors. These increases support the notion that dominantly westward drifting ring current ions are injected deeper into the inner magnetosphere under elevated geomagnetic activity [*Cornwall*, 1965; *Criswell*, 1969; *Jordanova et al*., 2001; *Fraser et al*., 2010]. The predawn sector ($200 < \text{MLT} \leq 400$) at $L > 6$ also features very high occurrence rates.

3.3. EMIC Waves by Solar Wind Dynamic Pressure

The dwell time of the Van Allen Probes has also been categorized based on the solar wind dynamic pressure experienced during the first precession of the mission. Dynamic pressure has been divided into two ranges: low-pressure values (Pdyn $\leq$ 3 nPa) and high-pressure values (Pdyn $>$ 3 nPa). These two distinctions were chosen after exploring other pressure ranges and were found to produce distinguishable spatial distributions. Figure 6 shows the dwell time of the Van Allen Probes with respect to the aforementioned dynamic pressure distinctions. Unlike the previous geomagnetic index dwell time plots, the dynamic pressure data coverage plots showcase an uneven distribution between low and high pressure. Figure 6a shows the data coverage for low-pressure conditions during the first precession of the Van Allen Probes. The high-pressure data coverage plot only features large (>1000 min) at the Van Allen Probes apogee. Regions encased below $L < 6$ have dwell times on the order of ~20–100 min. Here the "sufficient" dwell time coverage limit has been lowered to 40 min, i.e., the regions above $L = 4$. Occurrence rates against the total dwell time are not calculated.

Table 3. EMIC Wave Occurrence by Pressure Condition

	Pdyn [0,3] nPa	Pdyn (3,∞) nPa
Number of events	594	177
Hours of EMIC activity	350.31	80.28

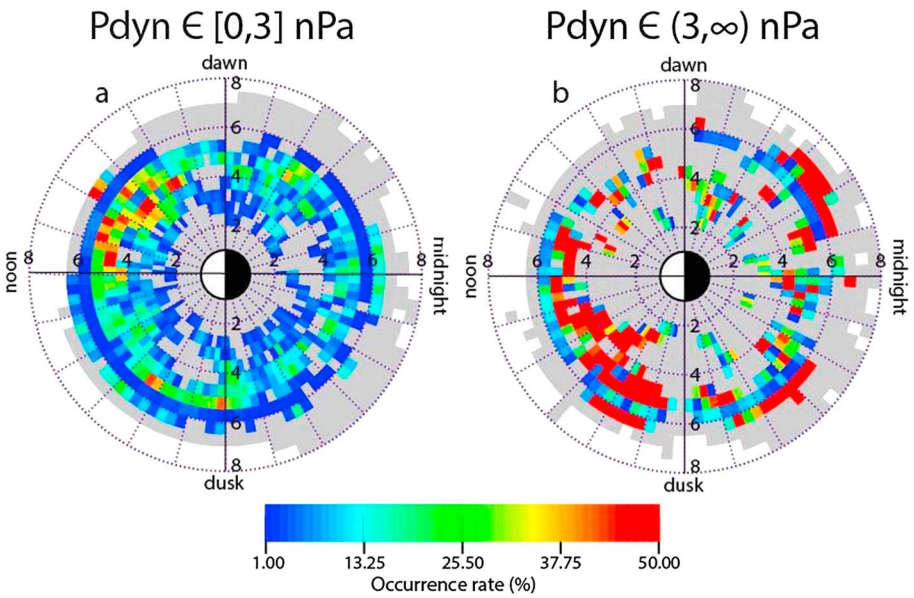

Figure 7. Same format as in Figure 6 but showing the occurrence rates of all EMIC waves observed by the Van Allen Probes under the pressure condition in which they were observed.

Table 3 shows the distribution of EMIC wave events observed using the low/high-pressure metric. Figure 7 shows the occurrence rates for both the low- and high-pressure EMIC wave events (Figures 7a and 7b, respectively). A majority of EMIC waves were observed during low solar wind pressures (594 EMIC wave events, ~350 h of EMIC wave activity). Consistent with the previous geomagnetic indices, the prenoon ($800 < \mathrm{MLT} \leq 1200$) sector at $L > 4$ features high occurrence rates ($>$ ~35%). Furthermore, the dayside of the magnetosphere generally has higher occurrence rates than compared to the nightside magnetosphere. EMIC wave events are observed in all MLT sectors.

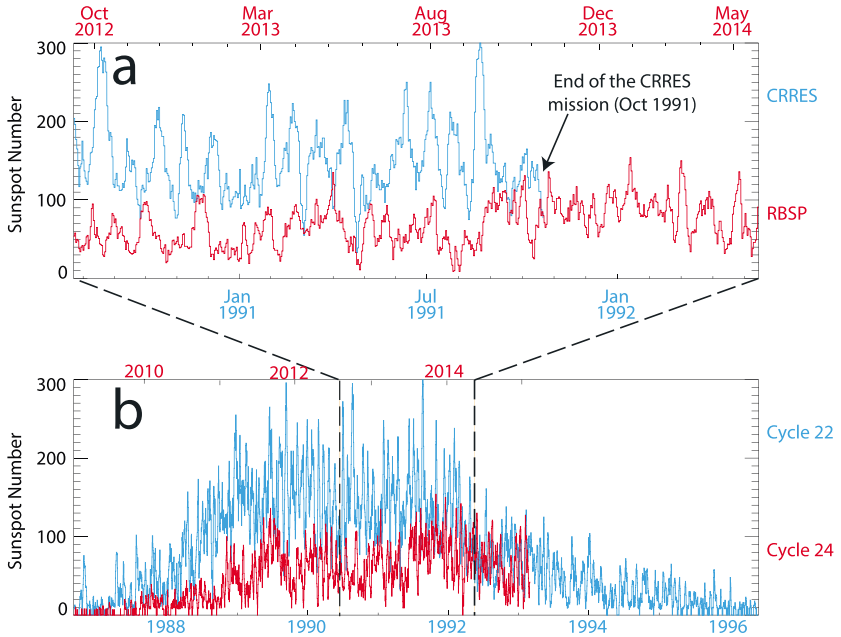

Figure 8. The total sunspot numbers observed (a) during the duration of the CRRES and Van Allen Probes' missions and (b) the total sunspot number observed during the solar cycles that coincide with the CRRES and the Van Allen Probes missions. Black dashed lines mark where Figure 8a coincides with Figure 8b.

Figure 7b shows the spatial distribution of EMIC waves observed during high-pressure times. Few EMIC wave events are observed during high-pressure times (177 EMIC wave events, ~104 h of EMIC wave activity). Occurrence rates increase on the dayside as the *L* shell decreases. However, this may be a symptom of insufficient dwell time. EMIC wave observations are primarily confined to the dayside magnetosphere, with an enhancement in the afternoon sector. High solar wind pressure does not produce increased spatial observations of inner magnetosphere EMIC waves on the nightside magnetosphere. The nightside does feature higher occurrence rates under high-pressure conditions than under low pressure. Increases in dynamic pressure are correlated with increased outer ($L > 7$) dayside and dawn sector magnetosphere EMIC wave occurrence rates [*Usanova et al*., 2012]. Unlike the outer magnetosphere, the inner magnetosphere does not feature increased observations of EMIC waves in the dawn sector.

3.4. Geomagnetic Activity and Solar Wind Data Coverage Comparison

Throughout each index used in this study, a disproportionate amount of dwell time has occurred when geomagnetic activity or solar wind dynamic pressure was considerably quiet or low. Using the methodology provided by *Halford et al.* [2010], we have found that 73 geomagnetic storms have occurred, as determined by *SYM-H*, during the first precession of the Van Allen Probes. *Halford et al.* [2010] found that 119 geomagnetic storms occurred during the entire duration of the CRRES mission. Furthermore, a majority of the EMIC wave events observed by CRRES during storm time were observed during the storm main phase. Despite having similar orbits to the CRRES mission, the Van Allen Probes observe more storm time EMIC wave events in the storm recovery phase. The discrepancy between both missions in regards to geomagnetic activity and by extension the observation of EMIC waves may be associated with the solar activity levels in their respective solar cycles.

Figure 8a shows the total number of sunspots observed for the first precession of the Van Allen Probes (displayed in red) and for the whole duration of the CRRES mission (displayed in blue). Consistently throughout the entirety of the CRRES mission, more sunspot activity was observed than the current Van Allen Probes era. Observations during the Van Allen Probes mission rarely exceeded a total sunspot number of 100. The CRRES era sunspot observations were consistently above 100, with total observations reaching as high 300 sunspots. The CRRES mission coincided with a more active solar cycle. Figure 8b shows the total sunspot number for solar cycle 22 (displayed in blue) and solar cycle 24 (displayed in red), which are the solar cycles for the CRRES and Van Allen Probes missions, respectively. Black dashed lines reflect where the CRRES and Van Allen Probe missions occurred during their respective solar cycles. Overall, solar cycle 22 was consistently more active than solar cycle 24. Lower solar activity decreases the amount of storm time intervals [*Gonzalez et al*., 1994; *Usanova et al*., 2012; *Keika et al*., 2013]. EMIC wave observations made by THEMIS also coincide with solar cycle 24, with *Usanova et al.* [2012] commenting about difficulties in generating statistics for high solar wind pressure conditions.

4. Discussion

Using observations from the first full MLT precession of the Van Allen Probes (the first 22 months of the mission), the spatial distributions of EMIC wave events have been examined under several geomagnetic indices and solar wind dynamic pressures. The occurrence rates of the inner magnetosphere EMIC wave events have been calculated with respect to various levels of the *AE* index, storm phase, and solar wind dynamic pressure. This survey serves as an extension to previous studies in which how the spatial distribution of EMIC waves change under different conditions over various magnetospheric regions is explored [*Kasahara et al*., 1992; *Halford et al*., 2010; *Usanova et al*., 2012; *Keika et al*., 2013; *Meredith et al*., 2014]. This study also expands upon previous statistical studies that investigate inner magnetosphere EMIC waves [*Saikin et al*., 2015; *Wang et al*., 2015; *Yu et al*., 2015] by examining geomagnetic conditions associated with the wave observations.

4.1. Geomagnetic Activity

It was reported in previous studies that the afternoon sector is the preferred region for EMIC wave observations [*Thorne*, 2010]. This region of the magnetosphere coincides with where plasmaspheric plumes are normally observed, which provides the cold ion populations necessary for EMIC wave growth. *Usanova et al.* [2013] reported that EMIC waves in the plasmaspheric plumes were ~20 times more likely to be

Table 4. Comparisons of EMIC Wave Statistical Studies by Geomagnetic Indices and Pdyn Used

Study	Spacecraft	*L* Range	MLT Range	Index	Key Results
Keika et al. [2013]	AMPTE CCE	3–9	All	*Dst*	Negative (positive) *Dst* values yield higher afternoon (dayside and dawn sector) occurrence rates. Main and recovery phase EMIC waves observed in the afternoon sector.
Kasahara et al. [1992]	Akebono	1–3	0–22, 23–24	*Kp*	Higher *Kp* values yield higher occurrence rates.
Halford et al. [2010]	CRRES	3–8	14–24, 0–8	*SYM-H*	Main and recovery phase EMIC waves observed in the afternoon sector.
Meredith et al. [2014]	CRRES	3–8	14–24, 0–8	*AE*	Disturbed *AE* values yield higher afternoon sector occurrence rates.
Usanova et al. [2012]	THEMIS	3–14	All	Pdyn	Dayside (dawn) occurrence rates increase for Pdyn $>$ 2 nPa (Pdyn $>$ 3 nPa).
				AE	Disturbed geomagnetic conditions yield high afternoon sector occurrences rates.
				SYM-H	Positive (negative) *SYM-H* values yield high EMIC occurrence rates in the afternoon and dawn (afternoon) sectors.
This study	Van Allen Probes	2–8	All	*AE*	Low (high) *AE* values yield prenoon (afternoon) occurrence peaks.
				SYM-H	Nonstorm (main and recovery phase) EMIC waves observed in the prenoon (afternoon) sector.
				Pdyn	Low (high) pressure yield higher prenoon (dayside) occurrence rates.

observed than an EMIC wave event outside them. During geomagnetic storms or substorms, energetic ring current particles can be injected deeper into the inner magnetosphere where they may overlap with the cold plasmasphere populations [*Cornwall*, 1965; *Jordanova et al.*, 2001]. In response to the storm, the plasmapause contracts and then expands in the storm recovery phase (and after the storm activity). *Saikin et al.* [2015] used the plasmapause model developed by *Moldwin et al.* [2002] which incorporates the *Kp* index to calculate a theoretical plasmapause location. In this study, an average plasmapause position of $L \approx 4.5$ and the highest EMIC wave occurrence regions located beyond this boundary are determined.

Overall, the storm time (by *SYM-H*) and the geomagnetic disturbed activity (by *AE*) EMIC wave events were preferentially observed in the afternoon sector beyond the $L \approx 4.5$ plasmapause boundary derived by *Saikin et al.* [2015]. Since the afternoon sector contains the highest occurrence rates during these periods, the hot ring current ions are able to overlap with the cold dense plasmasphere or plasmaspheric plumes. The appearance of higher occurrence rates at low *L* shells ($L < 4$) suggests that ring current ions are injected into the lower *L* shells. The occurrence peaks located in the afternoon sector also overlap with the location of the enhanced EMIC wave region where more intense EMIC wave events are observed [*Thorne*, 2010; *Saikin et al.*, 2015]. A majority of the storm time EMIC wave events were observed during the recovery phase of the storm, which may be due to the larger amount of dwell time. However, the larger amount of dwell time does not yield a higher overall occurrence rate. Unlike the main and recovery phases, the preonset phase has the lowest amount of dwell time because of the selected 3 h duration period (totaling 219 h) yet has the highest overall occurrence rate (7.9%). Since the main and recovery phases can last for longer time periods, the overall occurrence rate can be diminished when EMIC wave events are not observed by the Van Allen Probes. The preonset phase is also subject to this observational limitation; however, the relatively low number of storms (compared to *Halford et al.* [2010]) is most likely the cause. Furthermore, nonstorm time EMIC wave events constitute ~56% of total EMIC wave observations with the highest occurrence rates observed beyond $L \geq 4$ on the dayside magnetosphere. This survey also reveals the existence of a prenoon sector occurrence peak during both nonstorm time and when the geomagnetic activity is considered quiet. Low-energy ($<$100 eV) anisotropic ion drift may contribute to the excitation of EMIC wave events observed in this region and the overall dayside magnetosphere [*Anderson et al.*, 1996; *Yu et al.*, 2015].

4.2. Solar Wind Dynamic Pressure

Magnetopsheric compression-induced EMIC waves are primarily observed near the noon MLT sector at higher *L* shells [*Anderson and Hamilton*, 1993; *McCollough et al.*, 2010, 2012; *Usanova et al.*, 2012]. During compression events (i.e., high Pdyn), the magnetic field experiences the largest relative change in field strength around noon at higher *L* shells. These disruptions in the magnetic field can cause plasma to become unstable with particles executing the Shabansky orbits at middle to high MLATs [*Shabansky*, 1971; *McCollough et al.*, 2012; *Allen et al.*, 2015]. Therefore, the plasma becomes more favorable for EMIC wave generation [*Anderson and Hamilton*, 1993].

Most EMIC wave observations coincide with low-pressure (Pdyn $\leq$ 3 nPa) conditions. The results are consistent with the previous indices; that is, observations of EMIC wave events observed during low-pressure conditions have an occurrence peak in the prenoon ($800 < \text{MLT} \leq 1200$) region for $L > 4$. Unlike the quiet geomagnetic activity condition or the nonstorm time, low-pressure EMIC wave events are more spatially diverse in MLT at the lower L shells ($L < 4$). Furthermore, the Van Allen Probes' orbit does not exceed 20° MLAT and therefore does not primarily observe the off-equator source regions in the outer magnetosphere described in *Allen et al.* [2013] and *Allen et al.* [2015]. Simulations further show that inner magnetosphere proton anisotropies attributed to the Shabansky orbits are significantly lower than regions in the off-equator outer magnetosphere [*McCollough et al.*, 2012]. This discrepancy between the inner and outer magnetosphere suggests that outer magnetosphere EMIC waves are more susceptible to generation by dynamic pressure enhancements than their inner magnetosphere EMIC wave counterparts. Despite there being a limited number of high-pressure EMIC wave events, they are primarily observed throughout the dayside magnetosphere, especially the afternoon sector. The nightside magnetosphere features higher occurrence rates of high-pressure EMIC wave events than low-pressure events.

4.3. Comparison with Previous Studies

Previous statistical studies examined the relationship between EMIC wave events against geomagnetic activity levels and solar wind conditions. Each previous study has incorporated observations using different spacecraft to help form a complete global description of EMIC wave events in the Earth's magnetosphere. The previous studies, along with this study, have compiled data observations from August 1984 to June 2014. The study, spacecraft used, the MLT covered, the L shells observed, and the general results with respect to the geomagnetic index/Pdyn examined in each of those studies can be found in Table 4 (listed in order of spacecraft launch date).

As mentioned above, the CRRES mission coincided with the occurrence of 119 geomagnetic storms. Observations from the first precession of the Van Allen Probes have only coincided with 73 geomagnetic storms. Both missions are separated in time by ~20 years and therefore occurred during different solar cycles. Table 4 reveals that the selected previous statistical studies cover ~30 years, transcending solar cycle 21 to solar cycle 24. Higher solar activity in a solar cycle can impact the geomagnetic activity in the Earth's magnetosphere and likewise produce more geomagnetic storms which favor EMIC wave generation as described above. This study shows that the Van Allen Probes have significantly less storm time dwell time in the afternoon and postdawn sectors than the prenoon and premidnight sectors. This uneven dwell time coverage distribution during storm time may be explained by the strength of solar cycle 24. Solar cycle 24 has fewer total sunspots observed than solar cycle 22. Furthermore, dynamic pressure measurements over the past solar cycle have decreased [*McComas et al.*, 2013], which can also explain the uneven distribution of the low- and high-pressure dwell time coverage. When one compares EMIC wave statistical studies from older missions, the strength of the solar cycle associated with that respective mission should also be considered when performing that analysis.

Consistent throughout *Halford et al.* [2010], *Usanova et al.* [2012], *Keika et al.* [2013], *Meredith et al.* [2014], and this study is how the afternoon sector becomes more prominent with EMIC wave activity during disturbed geomagnetic activity or storm time. This study has adopted the same definitions of geomagnetic activity levels (i.e., quiet, moderate, and disturbed) as both *Usanova et al.* [2012] and *Meredith et al.* [2014]. Despite examining higher L shells than the Van Allen Probes ($L \geq 7$), THEMIS observes the same increase of EMIC wave observation as the *AE* index increases in the afternoon sector. The CRRES mission found peak EMIC wave occurrence rates (as high as 10%) in the inner magnetosphere under disturbed geomagnetic activity. Our results with regards to how disturbed *AE* values impact the afternoon sector are consistent with these previous studies.

The spatial distributions of EMIC waves observed between CRRES, THEMIS, and the Van Allen Probes are not consistent when examined with respect to quiet geomagnetic activity. First, throughout all MLT sectors, the CRRES mission observes very few EMIC wave events during quiet *AE* values [*Meredith et al.*, 2014]. However, the CRRES mission ended before any measurements of the 800–1400 MLTs could be collected. Therefore, a comparison of the prenoon ($800 < \text{MLT} \leq 1100$) occurrence peak during quiet activity with respect to EMIC wave events reported in this study cannot be performed with the work of *Meredith et al.* [2014]. At higher L shells ($L > 6.5$), quiet *AE* values did not produce increased wave observations in the prenoon sector.

The dawn-centered EMIC wave occurrence peak observed by THEMIS is more strongly correlated with magnetospheric compressions. Using both dynamic pressure and *SYM-H*, *Usanova et al.* [2012] found that the

occurrence rates of EMIC waves in the dawn sector decrease/increase depending on the index's value. High-pressure (Pdyn > 3 nPa) and positive *SYM-H* values (>10 nT), which correspond to magnetospheric compression, yielded higher occurrence rates of EMIC waves in the dawn sector compared to lower pressures and negative *SYM-H* values [*Usanova et al.*, 2012]. Inner magnetosphere EMIC wave event observations do not appear to be as sensitive to dynamic pressure increases like the outer magnetosphere. As mentioned above, this may be attributed to the inner magnetosphere not experiencing significant changes in magnetic field strength related to magnetospheric compressions to produce conditions favorable to EMIC wave generation. The Van Allen Probes also do not observe a dawn-centered EMIC wave occurrence peak [*Saikin et al.*, 2015].

Despite the AMPTE CCE and CRRES missions accumulating data from previous solar cycles, the spatial distributions of EMIC waves during storm times are consistent with our results. Using the same storm description as *Halford et al.* [2010], our study concurs with their work. That is, the afternoon sector produces more EMIC wave activity during the main and recovery phases. The CRRES mission shows most storm time EMIC waves being observed at $r \approx 5$–$6.6\ R_E$ in the afternoon sector. These regions overlap with where the Van Allen Probes observe peak EMIC wave occurrences during storm time ($L = 4$–6.5). The peak occurrence regions for both H^+ and He^+ band EMIC waves, as observed by AMPTE CCE, were located in the $L = 7$–9 afternoon sector during storm time as determined by *Dst*. Occurrence rates at these *L* shells vary between 1 and 25% during both the main and recovery phases [*Keika et al.*, 2013]. Inner magnetosphere EMIC waves ($L \leq 6$) observed by AMPTE CCE have lower occurrence rates (0–~15%). This discrepancy may be attributed to the different spatial coverage by AMPTE CCE and the Van Allen Probes.

This study and that by *Halford et al.* [2010] are consistent with respect to the overall distribution between nonstorm and storm time EMIC wave events. *Halford et al.* [2010] reports that 58% of total EMIC wave events observed occurred during no geomagnetic storm activity. For the first precession of the Van Allen Probes, 56% of total EMIC wave observations were found to coincide with no storm activity. However, our results found that storm time EMIC wave events were more often observed in the recovery phase of a geomagnetic storm than the main phase (see Table 2). This is in disagreement with the work by *Halford et al.* [2010], who found that the main phase contained more of the storm time EMIC wave observations. These results may be biased pending by the different solar activity levels in the two solar cycles. Since solar cycle 22 was predominately more active than solar cycle 24, more geomagnetic storms could be generated to allow for more main phase observations. Furthermore, the CRRES mission, as explained above, did not have measurements in the prenoon sector where the Van Allen Probes observe peak EMIC wave occurrence rates during nonstorm times. This bias in data coverage between the CRRES and Van Allen Probes missions may account for the differences in the distributions between the main and recovery phase EMIC wave events.

Not reflected in our analysis is an examination with wave amplitude against *AE* levels, storm phase, and dynamic pressure. Throughout this study, all EMIC wave events included in this study were observed to have a minimum wave power amplitude of 0.01 nT^2/Hz. An increased wave power threshold can alter the spatial distribution under varying levels of geomagnetic activity [*Meredith et al.*, 2014], the different storm phases, and dynamic pressures. Wave power amplitude plots in this L versus MLT format, along with wave band separation statistics, have been previously examined [*Saikin et al.*, 2015]. An analysis incorporating various wave power thresholds against the aforementioned parameters will therefore be examined in future work.

5. Conclusions

In this study, we have performed a statistical analysis of EMIC wave events observed by the Van Allen Probes and compared those measurements against the geomagnetic activity and solar wind conditions. This study encompasses high-resolution magnetic field data taken by the Van Allen Probes' EMFISIS instrument during the first 22 months of the mission (i.e., September 2012–June 2014), which is the first full MLT precession of the mission. This analysis incorporates over 700 EMIC wave events and how their spatial distributions relate to *AE* levels, storm phase, and solar wind dynamic pressure. The results are summarized as follows:

1. During quiet *AE* levels ($AE \leq 100$ nT), there is an EMIC wave occurrence peak located in the prenoon sector (~800 < MLT ≤ ~1100) at $L \approx 5.5$. As *AE* values increase to disturbed levels ($AE > 300$ nT), the peak occurrence region shifts to the afternoon sector (1200 < MLT ≤ 1800) at $L = 4$–6. Occurrence rates increase at the lower *L* shells ($L \leq 4$) as *AE* values increase.

2. Only 73 geomagnetic storms occurred during the first precession of the Van Allen Probes with 44% of total EMIC wave observations occurring during storm phases. Peak occurrence regions for nonstorm time events coincide with the quiet *AE* level occurrence peak. Storm time EMIC wave peak occurrence regions are located in the afternoon sector. A majority of the storm time EMIC wave events are observed in the recovery phase of the storm. Higher occurrence rates are found at lower *L* shells ($L \leq 4$) during storm time.
3. EMIC wave events occurring under low pressure (Pdyn ≤ 3 nPa) are observed at all MLT sectors, with occurrence rates peaking around the prenoon sector. High-pressure (Pdyn > 3 nPa) EMIC wave events are predominately observed in the afternoon sector and exhibit higher occurrence rates in the lower *L* shells and the nightside magnetosphere.
4. The current solar cycle, solar cycle 24, is considerably less active than previous solar cycles (e.g., solar cycle 22). This may cause discrepancies between our present study and previous studies [*Halford et al*., 2010; *Usanova et al*., 2012; *Keika et al*., 2013].

Acknowledgments
Work at UNH was supported by NASA under grants NNX11AO82G and NNX15AF66G. This work was also supported by Iowa subcontract 1000556126 to UNH in support of the Van Allen Probes and EMFISIS/MAG instruments and by RBSP-ECT funding provided by JHU/APL contract 967399 under NASA's Prime contract NAS5-01072. Work at the University of Iowa was performed under support on JHU/APL contract 921647 under NASA's Prime contract NAS501072. The authors thank Van Allen Probes team members for Van Allen Probes data preparation and software development. A.A. Saikin thanks Lynn Kistler, Eric Lund, and Christopher Mouikis for their helpful discussion. A special thanks is also given to Robert Allen for the help in developing software routines. The data used in this study were obtained from the EMFISIS data directory at http://emfisis.physics.uiowa.edu and CDAWEB for the OMNI sunspot numbers, solar wind parameters, and geomagnetic indices.

References

Allen, R. C., J. C. Zhang, L. M. Kistler, H. E. Spence, R. L. Lin, M. W. Dunlop, and M. André (2013), Multiple bidirectional EMIC waves observed by Cluster at middle magnetic latitudes in the dayside magnetosphere, *J. Geophys. Res. Space Physics*, *118*, 6266–6278, doi:10.1002/jgra.50600.

Allen, R. C., J.-C. Zhang, L. M. Kistler, H. E. Spence, R.-L. Lin, B. Klecker, M. W. Dunlop, M. André, and V. K. Jordanova (2015), A statistical study of EMIC waves observed by Cluster: 1. Wave properties, *J. Geophys. Res. Space Physics*, *120*, 5574–5592, doi:10.1002/2015JA021333.

Anderson, B. J., and D. C. Hamilton (1993), Electromagnetic ion cyclotron waves stimulated by modest magnetospheric compressions, *J. Geophys. Res.*, *98*, 11,369–11,382, doi:10.1029/93JA00605.

Anderson, B. J., R. E. Erlandson, and L. J. Zanetti (1992), A statistical study of Pc 1-2 magnetic pulsations in the equatorial magnetosphere. I—Equatorial occurrence distributions, *J. Geophys. Res.*, *97*, 3075–3088, doi:10.1029/91JA02706.

Anderson, B. J., R. E. Denton, G. Ho, D. C. Hamilton, S. A. Fuselier, and R. J. Strangeway (1996), Observational test of local proton cyclotron instability in the Earth's magnetosphere, *J. Geophys. Res.*, *101*, 527–543, doi:10.1029/96JA01251.

Bräysy, T., K. Mursula, and G. Marklund (1998), Ion cyclotron waves during a great magnetic storm observed by Freja double-probe electric field instrument, *J. Geophys. Res.*, *103*, 4145–4155, doi:10.1029/97JA02820.

Cornwall, J. M. (1965), Cyclotron instabilities and electromagnetic emission in the ultra low frequency and very low frequency ranges, *J. Geophys. Res.*, *70*, 61–69, doi:10.1029/JZ070i001p00061.

Criswell, D. R. (1969), Pc 1 micropulsation activity and magnetospheric amplification of 0.2- to 5.0-Hz hydromagnetic waves, *J. Geophys. Res.*, *74*, 205–224, doi:10.1029/JA074i001p00205.

Engebretson, M. J., et al. (2013), Multi-instrument observations from Svalbard of a traveling convection vortex, electromagnetic ion cyclotron wave burst, and proton precipitation associated with a bow shock instability, *J. Geophys. Res. Space Physics*, *118*, 2975–2997, doi:10.1002/jgra.50291.

Engebretson, M. J., et al. (2015), Van Allen probes, NOAA, GOES, and ground observations of an intense EMIC wave event extending over 12 h in magnetic local time, *J. Geophys. Res. Space Physics*, *120*, 5465–5488, doi:10.1002/2015JA021227.

Fraser, B. J., W. J. Kemp, and D. J. Webster (1989), Ground-satellite study of a Pc 1 ion cyclotron wave event, *J. Geophys. Res.*, *94*, 855–863, doi:10.1029/JA094iA09p11855.

Fraser, B. J., and T. S. Nguyen (2001), Is the plasmapause a preferred source region of electromagnetic ion cyclotron waves in the magnetosphere? *J. Atmos. Sol. Terr. Phys.*, *63*, 1225–1247, doi:10.1016/S1364-6826(00)00225-X.

Fraser, B. J., R. S. Grew, S. K. Morley, J. C. Green, H. J. Singer, T. M. Loto'aniu, and M. F. Thomsen (2010), Storm time observations of electromagnetic ion cyclotron waves at geosynchronous orbit: GOES results, *J. Geophys. Res.*, *115*, A05208, doi:10.1029/2009JA014516.

Fuselier, S. A., S. P. Gary, M. F. Thomsen, E. S. Claflin, B. Hubert, B. R. Sandel, and T. Immel (2004), Generation of transient dayside subauroral proton precipitation, *J. Geophys. Res.*, *109*, 1–11, doi:10.1029/2004JA010393.

Gonzalez, W. D., J. A. Joselyn, Y. Kamide, H. W. Kroehl, G. Rostoker, B. T. Tsurutani, and V. M. Vasyliunas (1994), What is a geomagnetic storm?, *J. Geophys. Res.*, *99*, 5771, doi:10.1029/93JA02867.

Halford, A. J., B. J. Fraser, and S. K. Morley (2010), EMIC wave activity during geomagnetic storm and nonstorm periods: CRRES results, *J. Geophys. Res.*, *115*, A12248, doi:10.1029/2010JA015716.

Horne, R. B., and R. M. Thorne (1993), On the preferred source location for the convective amplification of ion cyclotron waves, *J. Geophys. Res.*, *98*, 9233–9247, doi:10.1029/92JA02972.

Jordanova, V. K., J. Albert, and Y. Miyoshi (2008), Relativistic electron precipitation by EMIC waves from self-consistent global simulations, *J. Geophys. Res.*, *113*, A00A10, doi:10.1029/2008JA013239.

Jordanova, V. K., C. J. Farrugia, R. M. Thorne, G. V. Khazanov, G. D. Reeves, and M. F. Thomsen (2001), Modeling ring current proton precipitation by electromagnetic ion cyclotron waves during the May 14–16, 1997, storm, *J. Geophys. Res.*, *106*, 7–22, doi:10.1029/2000JA002008.

Kasahara, Y., A. Sawada, M. Yamamoto, I. Kimura, S. Kokubun, and K. Hayashi (1992), Ion cyclotron emissions observed by the satellite Akebono in the vicinity of the magnetic equator, *Radio Sci.*, *27*(2), 347–362, doi:10.1029/91RS01872.

Keika, K., K. Takahashi, A. Y. Ukhorskiy, and Y. Miyoshi (2013), Global characteristics of electromagnetic ion cyclotron waves: Occurrence rate and its storm dependence, *J. Geophys. Res. Space Physics*, *118*, 4135–4150, doi:10.1002/jgra.50385.

Kennel, C. F., and H. E. Petschek (1966), Limits on stably trapped particle fluxes, *J. Geophys. Res.*, *71*, 1–28, doi:10.1177/1069072705283987.

Kessel, R. L., N. J. Fox, and M. Weiss (2013), The Radiation Belt Storm Probes (RBSP) and Space Weather, *Space Sci. Rev.*, *179*, 531–543, doi:10.1007/s11214-012-9953-6.

Kletzing, C. A., et al. (2013), The Electric and Magnetic Field Instrument Suite and Integrated Science (EMFISIS) on RBSP, *Space Sci. Rev.*, *179*, 127–181, doi:10.1007/s11214-013-9993-6.

Lockwood, M., S. W. H. Cowley, P. E. Sandholt, and R. P. Lepping (1990), The ionospheric signatures of flux transfer events and solar wind dynamic pressure changes, *J. Geophys. Res.*, *95*, 17,113–17,135, doi:10.1029/JA095iA10p17113.

Loto'aniu, T. M., B. J. Fraser, and C. L. Waters (2005), Propagation of electromagnetic ion cyclotron wave energy in the magnetosphere, *J. Geophys. Res.*, *110*, A07214, doi:10.1029/2004JA010816.

Lyons, L. R., R. M. Thorne, and C. F. Kennel (1972), Pitch-angle diffusion of radiation belt electrons within the plasmasphere, *J. Atmos. Sol. Terr. Phys.*, *77*, 3455–3474, doi:10.1029/JA077i028p05608.

Mauk, B. H., and R. L. McPherron (1980), An experimental test of the electromagnetic ion cyclotron instability within the Earth's magnetosphere, *Phys. Fluids*, *23*, 2111–2127, doi:10.1063/1.862873.

Mauk, B. H., N. J. Fox, S. G. Kanekal, R. L. Kessel, D. G. Sibeck, and A. Ukhorskiy (2013), Science objectives and rationale for the Radiation Belt Storm Probes mission, *Space Sci. Rev.*, *179*, 3–27, doi:10.1007/s11214-012-9908-y.

McCollough, J. P., S. R. Elkington, and D. N. Baker (2012), The role of Shabansky orbits in compression-related electromagnetic ion cyclotron wave growth, *J. Geophys. Res.*, *117*, A01208, doi:10.1029/2011JA016948.

McCollough, J. P., S. R. Elkington, M. E. Usanova, I. R. Mann, D. N. Baker, and Z. C. Kale (2010), Physical mechanisms of compressional EMIC wave growth, *J. Geophys. Res.*, *115*, A10214, doi:10.1029/2010JA015393.

McComas, D. J., N. Angold, H. A. Elliott, G. Livadiotis, N. A. Schwadron, R. M. Skoug, and C. W. Smith (2013), Weakest solar wind of the space age and the current "mini" solar maximum, *Astrophys. J.*, *779*(2008), 1–10, doi:10.1088/0004-637X/779/1/2.

Meredith, N. P., R. B. Horne, T. Kersten, B. J. Fraser, and R. S. Grew (2014), Global morphology and spectral properties of EMIC waves derived from CRRES observations, *J. Geophys. Res. Space Physics*, *119*, 1–15, doi:10.1002/2014JA020064.

Merka, J., A. Szabo, J. Safrankova, and Z. Nemecek (2003), Earth's bow shock and magnetopause in the case of a field-aligned upstream flow: Observation and model comparison, *J. Geophys. Res.*, *108*(A7), 1269, doi:10.1029/2002JA009697.

Min, K., J. Lee, K. Keika, and W. Li (2012), Global distribution of EMIC waves derived from THEMIS observations, *J. Geophys. Res.*, *117*, A05219, doi:10.1029/2012JA017515.

Moldwin, M. B., L. Downward, H. K. Rassoul, R. Amin, and R. R. Anderson (2002), A new model of the location of the plasmapause: CRRES results, *J. Geophys. Res.*, *107*, 1–9, doi:10.1029/2001JA009211.

Morley, S. K., S. T. Ables, M. D. Sciffer, and B. J. Fraser (2009), Multipoint observations of Pc1-2 waves in the afternoon sector, *J. Geophys. Res.*, *114,* A09205, doi:10.1029/2009JA014162.

Olson, J. V., and L. C. Lee (1983), Pc1 wave generation by sudden impulses, *Planet. Space Sci.*, *31*(3), 295–302, doi:10.1016/0032-0633(83)90079-X.

Pickett, J. S., et al. (2010), Cluster observations of EMIC triggered emissions in association with Pc1 waves near Earth's plasmapause, *Geophys. Res. Lett.*, *37*, L09104, doi:10.1029/2010GL042648.

Rauch, J. L., and A. Roux (1982), Ray tracing of ULF waves in a multicomponent magnetospheric plasma: Consequences for the generation mechanism of ion cyclotron waves, *J. Geophys. Res.*, *87*, 8191–8198, doi:10.1029/JA087iA10p08191.

Saikin, A. A., J.-C. Zhang, R. C. Allen, C. W. Smith, L. M. Kistler, H. E. Spence, R. B. Torbert, C. A. Kletzing, and V. K. Jordanova (2015), The occurrence and wave properties of H^+-, He^+-, and O^+-band EMIC waves observed by the Van Allen Probes, *J. Geophys. Res. Space Physics*, *120*, 1–16, doi:10.1002/2015JA021358.

Sakaguchi, K., K. Shiokawa, Y. Miyoshi, Y. Otsuka, T. Ogawa, K. Asamura, and M. Connors (2008), Simultaneous appearance of isolated auroral arcs and Pc 1 geomagnetic pulsations at subauroral latitudes, *J. Geophys. Res.*, *113*, A05201, doi:10.1029/2007JA012888.

Shabansky, V. P. (1971), Some processes in the magnetosphere, *Space Sci. Rev.*, *12*, 299–418, doi:10.1007/BF00165511.

Summers, D., B. Ni, and N. P. Meredith (2007), Timescales for radiation belt electron acceleration and loss due to resonant wave-particle interactions: 2. Evaluation for VLF chorus, ELF hiss, and electromagnetic ion cyclotron waves, *J. Geophys. Res.*, *112*, A04207, doi:10.1029/2006JA011993.

Summers, D., and R. M. Throne (2003), Relativistic electron pitch-angle scattering by electromagnetic ion cyclotron waves during geomagnetic storms, *J. Geophys. Res.*, *108*(A4), 1143, doi:10.1029/2002JA009489.

Thorne, R. M., and C. F. Kennel (1971), Relativistic electron precipitation during magnetic storm main phase, *J. Geophys. Res.*, *76*, 4446–4453, doi:10.1029/JA076i019p04446.

Thorne, R. M. (2010), Radiation belt dynamics: The importance of wave-particle interactions, *Geophys. Res. Lett.*, *37*, L22107, doi:10.1029/2010GL044990.

Tsurutani, B. T., and E. J. Smith (1977), Two types of magnetospheric ELF chorus and their substorm dependences, *J. Geophys. Res.*, *82*, 5112–5128, doi:10.1029/JA082i032p05112.

Tsyganenko, N. A., and M. I. Sitnov (2005), Modeling the dynamics of the inner magnetosphere during strong geomagnetic storms, *J. Geophys. Res.*, *110*, A03208, doi:10.1029/2004JA010798.

Usanova, M. E., I. R. Mann, J. Bortnik, L. Shao, and V. Angelopoulos (2012), THEMIS observations of electromagnetic ion cyclotron wave occurrence: Dependence on *AE*, *SYMH*, and solar wind dynamic pressure, *J. Geophys. Res.*, *117*, A10218, doi:10.1029/2012JA018049.

Usanova, M. E., F. Darrouzet, I. R. Mann, and J. Bortnik (2013), Statistical analysis of EMIC waves in plasmaspheric plumes from Cluster observations, *J. Geophys. Res. Space Physics*, *118*, 4946–4951, doi:10.1002/jgra.50464.

Wang, D., Z. Yuan, X. Yu, X. Deng, M. Zhou, S. Huang, H. Li, Z. Wang, C. A. Kletzing, and J. R. Wygant (2015), Statistical characteristics of EMIC waves: Van Allen Probe observations, *J. Geophys. Res. Space Physics*, *120*, 6199–6206, doi:10.1002/2015JA021354.Received.

Young, D. T., S. Perraut, A. Roux, C. de Villedary, R. Gendrin, A. Korth, G. Kremser, and D. Jones (1981), Wave-particle interactions near observed on GEOS 1 and 2 of ion cyclotron waves in He^+-rich plasma Max-Planck-Institut far Katlenburg-Lindau 3, made with the ESA/GEOS 1 and 2 spacecraft which give an purpose, *J. Geophys. Res.*, *86*, 6755–6772, doi:10.1029/JA086iA08p06755.

Yu, X., Z. Yuan, D. Wang, H. Li, S. Huang, Z. Wang, Q. Zheng, M. Zhou, C. A. Kletzing, and J. R. Wygant (2015), In situ observations of EMIC waves in O^+ band by the Van Allen Probe A, *Geophys. Res. Lett.*, *42*, 1312–1317, doi:10.1002/2015GL063250.

Zhang, J.-C., L. M. Kistler, C. G. Mouikis, M. W. Dunlop, B. Klecker, and J.-A. Sauvaud (2010), A case study of EMIC wave-associated He^+ energization in the outer magnetosphere: Cluster and Double Star 1 observations, *J. Geophys. Res.*, *115*, A06212, doi:10.1029/2009JA014784.

Zhang, J.-C., L. M. Kistler, C. G. Mouikis, B. Klecker, J. A. Sauvaud, and M. W. Dunlop (2011), A statistical study of EMIC wave-associated He^+ energization in the outer magnetosphere: Cluster/CODIF observations, *J. Geophys. Res.*, *116*, A11201, doi:10.1029/2011JA016690.

Zhang, J.-C., et al. (2014), Excitation of EMIC waves detected by the Van Allen Probes on 28 April 2013, *Geophys. Res. Lett.*, *41*, 4101–4108, doi:10.1002/2014GL060621.